Applied Catalysis B: Environmental 130–131 (2013) 277–284

Contents lists available at SciVerse ScienceDirect

Applied Catalysis B: Environmental

journal homepage: www.elsevier.com/locate/apcatb

Ordered mesoporous CeO_2-TiO_2 composites: Highly efficient photocatalysts for the reduction of CO_2 with H_2O under simulated solar irradiation

Yangang Wang[a,*], Bo Li[b], Chengli Zhang[b], Lifeng Cui[a], Shifei Kang[b], Xi Li[b,*], Lihui Zhou[c]

[a] School of Environment and Architecture, University of Shanghai for Science and Technology, Shanghai 200093, China
[b] Department of Environmental Science and Engineering, Fudan University, Shanghai 200433, China
[c] School of Chemistry and Molecular Engineering, East China University of Science and Technology, Shanghai 200237, China

ARTICLE INFO

Article history:
Received 12 August 2012
Received in revised form 25 October 2012
Accepted 11 November 2012
Available online 24 November 2012

Keywords:
Ordered mesoporous
CeO_2-TiO_2 composites
Nanocasting route
Photocatalyst
Reduction of CO_2

ABSTRACT

Ordered mesoporous CeO_2-TiO_2 composites with 2D hexagonal structure and varied compositions were synthesized through a nanocasting route using ordered mesoporous SBA-15 as the template. X-ray diffraction, nitrogen adsorption-desorption, transmission electron microscopy, X-ray photoelectron spectroscopy and UV-vis diffuse reflectance spectra analysis techniques were used to characterize the samples. It is observed that the obtained CeO_2-TiO_2 composites have ordered 2D hexagonal mesostructures with high specific surface area and hierarchical porosity. Introduction of CeO_2 species can effectively extend the spectral response from UV to visible area and enhance the surface chemisorbed oxygen of the ordered mesoporous TiO_2. Due to the peculiar composition and structural characteristics, these ordered mesoporous CeO_2-TiO_2 composites exhibited excellent photocatalytic activity in the reduction of CO_2 with H_2O under simulated solar irradiation.

1. Introduction

The increasing atmospheric concentration of carbon dioxide (CO_2) due to fossil fuel combustion has raised serious concerns about global warming [1,2]. Solar photocatalytic conversion of CO_2 with H_2O into hydrocarbon fuels by semiconductors has sparked a new sustainable development path since it would help reduce atmospheric CO_2 levels and partly fulfill energy demands [3–5]. Among various oxide semiconductor photocatalysts, TiO_2 is one of the most common one due to its powerful oxidation properties, non-toxicity, low cost and long-term photostability [6–8]. However, the activity of pure TiO_2 in the photocatalytic reduction of CO_2 with H_2O is not high enough for practical use. To increase the photoactivity of TiO_2, several approaches have been suggested, such as reducing particle size [8,9], loading of metal [10–14], and dispersing on various supports [5,15–18]. These approaches have resulted in improvements of the catalytic performance of TiO_2-based photocatalysts but only to a limited extent. Recent progress shows that TiO_2 coupled with other semiconductors with suitable matching of band levels, like SnO_2 [19–22], WO_3 [23–25], CdS [26–28], Fe_2O_3 [29,30], CeO_2 [31,32], and ZrO_2 [33], can greatly increase the photocatalytic efficiency by increasing the charge separation and extending the energy range of photoexcitation. Among them, CeO_2-TiO_2 composite is one of the most promising since the introduction of CeO_2 not only maintains their original structural features but also endows the resultant composite with additional properties [34,35].

In recent years, ordered mesostructures of metal oxides and their composites have attracted a great deal of attention due to their peculiar properties and wide potential applications [36]. Design of photocatalysts with well-defined mesoporous structure is a promising way to achieve high photocatalytic activity since the ordered mesopore channels facilitate fast intraparticle molecular transfer. While the large surface area may enhance the light harvesting and the adsorption for reactant molecules [37]. Although ordered mesoporous TiO_2 has already been widely investigated, only limited studies have been performed on the ordered mesoporous TiO_2 coupled semiconductor photocatalysts, especially for CeO_2-TiO_2 system. Recently, Yu et al. [38] reported the synthesis of ordered mesoporous CeO_2 doped TiO_2 photocatalyst (Ce/Ti molar ratio = 0.05) by an evaporation-induced self-assembly (EISA) method, their result showed the doping CeO_2 species into TiO_2 framework not only improve the thermal stability of the ordered mesoporous structure but also effectively extend the photo-response of TiO_2 to the visible-light region. However, to the best of our knowledge, there is no report on the synthesis of the ordered mesoporous CeO_2-TiO_2 composites with varied compositions and their activity toward photocatalytic CO_2 reduction.

In this work, we report a new approach to prepare ordered mesoporous CeO_2-TiO_2 composites with 2D hexagonal structure

* Corresponding authors. Tel.: +86 21 55275979; fax: +86 21 55275979.
E-mail addresses: ygwang8136@gmail.com (Y. Wang), xi_li@fudan.edu.cn (X. Li).

0926-3373/$ – see front matter © 2012 Elsevier B.V. All rights reserved.
http://dx.doi.org/10.1016/j.apcatb.2012.11.019

and varied compositions based on the nanocasting route. The synthesis was achieved using ordered mesoporous SBA-15 as a template, titanium tetrachloride and cerium nitrate were respectively used as the Ti source and Ce precursor. The structural properties of the obtained materials were analyzed by X-ray diffraction (XRD), nitrogen adsorption-desorption, transmission electron microscopy (TEM), X-ray photoelectron spectroscopy (XPS) and UV-vis diffuse reflectance spectra (UV-vis), their photocatalytic activity was examined toward the reduction of CO_2 with H_2O under simulated solar irradiation. It was found that the induced CeO_2 significantly enhanced the photoactivity of ordered mesoporous TiO_2. To the best of our knowledge, this is the first time to report the enhanced photoactivity of ordered mesoporous CeO_2-TiO_2 composites to the reduction of CO_2 with H_2O.

2. Experimental

2.1. Chemicals

Pluronic P123 (Mw = 5800, $EO_{20}PO_{70}EO_{20}$) was purchased from Aldrich. Tetraethoxysilane (TEOS), hydrochloric acid, glycerol, sodium hydroxide, acetone, cerium nitrate hexahydrate ($Ce(NO_3)_3{\cdot}6H_2O$), and titanium tetrachloride ($TiCl_4$) were purchased from Shanghai Chemical Corp. All chemicals were used as received without further purification.

2.2. Catalyst preparation

Ordered mesoporous silica SBA-15 template with rod-like morphology was synthesized as the reported procedure except enlarging the amount by ten times [39]. Ordered mesoporous CeO_2-TiO_2 composites were synthesized using the hard template method with the help of acetone. In a typical preparation process, a total 12 mmol of $TiCl_4$ and $Ce(NO_3)_3{\cdot}6H_2O$ with different Ce/Ti molar ratios (0.5, 1.0, 2.0) in sequence was dissolved into 15 mL of acetone. After the solution became clear, 2 g of SBA-15 hard template was added and the mixture was stirred for 2 hours in a 100 mL beaker, then the mixture was transferred to a clean flat Petri dish (diameter: 8 cm) and the solvent was evaporated. In order to achieve higher loadings, the above dried hybrid powder was calcined at 200 °C for 6 h to decompose the metal precursors, and then the impregnation step was repeated, but the amount of precursors was reduced to 2/3 compared to the first step. The resulting samples were calcined in air at 500 °C for 4 h with a heating ramp of 1 K min^{-1} to completely decompose the inorganic precursors. Finally, the silica template was removed using a 2 M NaOH aqueous solution at room temperature and this etching process was repeated three times. The obtained CeO_2-TiO_2 composites with different initial Ce/Ti molar ratios (0.5, 1.0, 2.0) are denoted as Mes-CeTi-0.5, Mes-CeTi-1.0, and Mes-CeTi-2.0, respectively. For comparison, ordered mesporous TiO_2 (Mes-TiO_2) and mesoporous CeO_2 (Mes-CeO_2) were also prepared by the same method.

2.3. Catalyst characterization

Low-angle X-ray diffraction patterns were collected in θ-2θ mode using Rigaku D/MAX-2550VB/PC diffractometer ($CuK\alpha_1$ radiation, λ=1.5406 Å), operated at 40 kV and 200 mA (scanning step: 0.02° per second). Wide-angle XRD patterns were collected in the same mode, but operated at 100 mA. Transmission electron microscope (TEM) images were done using a JEOL JEM-2010 electron microscope with an acceleration voltage of 200 kV. Nitrogen sorption isotherms were measured at -196 °C on a Micromeritics ASAP 2000 apparatus. The diffuse reflectance spectra of the samples over a range of 200-800 nm were recorded by a Varian Cary 500 Scan UV-vis system. X-ray photoelectron spectroscopy (XPS) measurement was carried out on a RBO upgraded PHI-5000 C ESCA system (Pekin Elmer) using monochromated Al Kα X-rays (hν=1486.6 eV) as a radiation at 250 W. All binding energies were calibrated by using the contaminant carbon (C_{1S} = 284.6 eV) as a reference.

2.4. Photocatalytic performance tests

Photocatalytic activity tests for the reduction of CO_2 with H_2O were carried out in a stainless steel reactor with the volume of 1500 ml (as shown in Fig. 1). Catalyst powder (0.10 g) was dispersed on the stainless steel omentum which was fixed in the center of reactor. The bottom of glass wool support was moisturized with 5.0 g of deionized water to maintain saturated water vapor in the reactor, and a Xe arc lamp (300 W) with sunlike radiation spectrum was put at the top of quartz window with the distance of 8 cm, which can irradiate the whole catalyst powder. In order to control the reaction temperature, the Xe lamp was placed in a cold trap and the whole reactor system is in the air circulation. Prior to illumination, the reactor was first purged with the $CO_2 + H_2O$ mixture at 100 mL/min for 2 h and then reduced to 20 mL/min for another 1 h to establish an adsorption-desorption balance, and the gas phase volume concentrations of CO_2 and H_2O were controlled at about 95.5% and 4.5%, respectively. After that, the reactor was tightly closed and the Xe lamp was then switched on to start the experiment. The reaction temperature and pressure were maintained at 30 °C and 110KPa, respectively. The gas phase products were taken at various time during the irradiation and analyzed by gas chromatography.

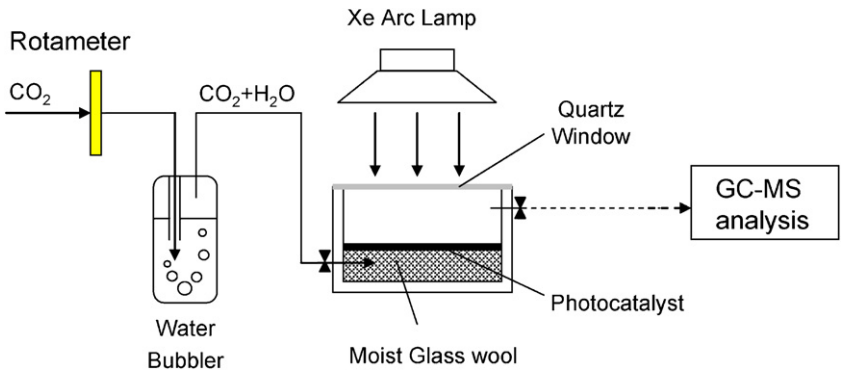

Fig. 1. Schematic of experimental setup for the photocatalytic reduction of CO_2 with H_2O.

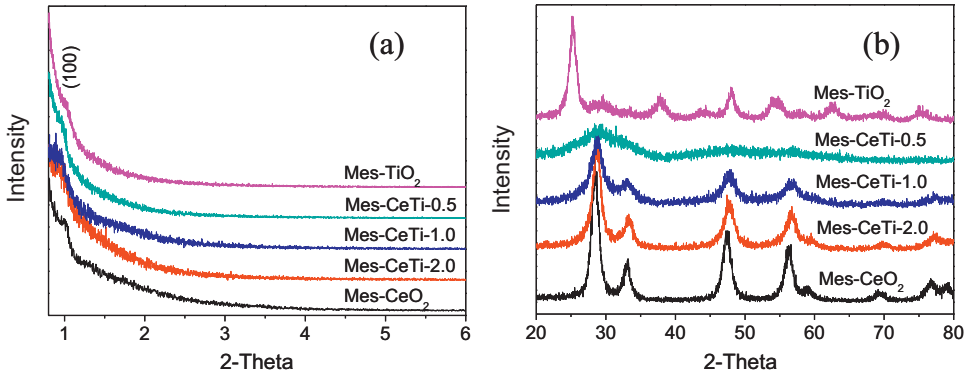

Fig. 2. Low-angle (a) and wide-angle (b) XRD patterns of Mes-TiO_2, Mes-CeTi-0.5, Mes-CeTi-1.0, Mes-CeTi-2.0, and Mes-CeO_2.

3. Results and discussion

3.1. Characteristics of catalysts

The formation of ordered mesoporous CeO_2-TiO_2 composites with different compositions is firstly provided by XRD analysis as shown in Fig. 2. The low-angle XRD patterns in Fig. 2a show that a moderate diffraction corresponding to (100) reflection of the 2D hexagonal (*p*6*mm*) symmetry can be observed for all samples, indicating the synthesized CeO_2-TiO_2 composites have retained some regular mesostructures although the higher angle two diffractions indexed to (110) and (200) are too weak to be detected, as confirmed by their TEM images (see below). Fig. 2b shows the wide-angle XRD patterns, it can be seen that in addition to an anatase structure observed for pure TiO_2, the structures of pure CeO_2 and other three CeO_2-TiO_2 composites were identified as cubic fluorite phase. It should be noted that the peaks of cubic fluorite phase become broader and the intensity becomes weaker with the decreasing content of CeO_2 in the composites, and sample Mes-CeTi-0.5 with the lowest of Ce/Ti molar ratio exhibits a very broad diffraction peak at 2θ=24-37° which is ascribed to the overlap of two peaks, indicating amorphous-like structure. The intensity difference and peak broadening of the CeO_2-TiO_2 composites were attributed to a significant reduction of crystallite size. In addition, the peaks corresponding to cubic fluorite phase of composites are shifted toward lower angle with increasing CeO_2 content because of the larger ionic radius of Ce^{4+} (0.97 Å) than Ti^{4+} (0.61 Å). Energy dispersive X-ray (EDX) analysis showed that the molar ratio of the residual Si in these ordered mesoporous CeO_2-TiO_2 composites was very low (Table 1), indicating most of the silica template has been removed.

The nitrogen adsorption/desorption isotherms and pore size distribution curves of above samples are shown in Fig. 3. All isotherm curves show an obvious uptake of N_2 as a result of capillary condensation in a wide relative pressure (P/P_0) range of 0.55-0.95, which indicates the existence of multiform pore distributions. The pore size distribution obtained from an analysis of desorption branch of the isotherms is shown in Fig. 3b. It can be seen that except Mes-TiO_2 with a relative broad pore size distribution, other four samples possess bimodal pore size distributions centered at about 3.3 and 9.1 nm which are respectively ascribed to the dissolution of the silica walls and the coalescence of unfilled spaces of the template SBA-15 or/and the voids between the small particles. The corresponding textural properties are summarized in Table 1. These ordered mesoporous materials generally have high BET surface areas (134.6-254.1 m^2/g) and large pore volumes (0.515-0.832 cm^3/g), and both are increased with the decrease of CeO_2 content in composites.

Fig. 4 shows the TEM images of the Mes-TiO_2, Mes-CeTi-0.5, Mes-CeTi-1.0, Mes-CeTi-2.0, and Mes-CeO_2. From the low-magnification TEM images (Fig. 4 left), it can be seen that besides the rodlike morphology, ordered 2D hexagonal mesostructure can be clearly observed for all samples, suggesting thus-prepared materials are well reverse-replica of the template, which is consistent with low-angle XRD results. The high resolution TEM (HRTEM) images in Fig. 4 right show the detail structure of the mesopores, and the pore walls are well constituted by metal oxide nanocrystals with a diameter of several nanometers. The selected area electron diffraction (SAED) patterns are given in the inset of Fig. 4 left. All shows the diffraction rings, indicating that the metal oxide nanocrystals, as building units of the pore walls, are polycrystalline. It should be noted that the diffraction rings for Mes-CeTi-0.5 are not very clear since the semicrystalline structure, which is in agreement with its wide-angle XRD result.

In order to investigate the electronic states of the catalysts, UV-vis diffuse reflectance spectroscopy (DRS) studies were performed on Mes-TiO_2, Mes-CeTi-0.5, Mes-CeTi-1.0, Mes-CeTi-2.0, and Mes-CeO_2 (as shown in Fig. 5). For comparison, a commercial titania powers P25 was also measured and plotted in same Figure. Interestingly, the Mes-TiO_2 displays a slight red shift of light absorption with respect to the commercial P25 which absorbs light with wavelength shorter than 400 nm, this is phenomenon may ascribed to its ordered mesoporous structure, enlarged surface area and multiple scatting enable it to harvest light much more efficiently [40]. The samples of three ordered mesoporous CeO_2-TiO_2 composites show spectral response in a broad visible region (λ = 400-600 nm) owing to the photosentisizing effect of CeO_2. It is worthy to note that these CeO_2-TiO_2 composites exhibit a much stronger absorption in both untraviolet and visble-light regions than that of Mes-TiO_2, this enhanced light-trapping effect is the result of the reflection

Table 1
Textural properties and the energy of band gap (E_g) of Mes-TiO_2, Mes-CeTi-0.5, Mes-CeTi-1.0, Mes-CeTi-2.0, and Mes-CeO_2.

Sample	Ce:Ti molar ratio	Ce:Ti molar ratio (XPS)	Surface area (m^2/g)	Pore size (nm)	Pore volume (cm^3/g)	Residual Si (mol%)	E_g (eV)
Mes-TiO_2	0:1	–	254.1	5.4	0.832	1.4	2.81
Mes-CeTi-0.5	1:2	1:2.08	182.4	3.3, 9.1	0.611	1.3	2.16
Mes-CeTi-1.0	1:1	1:0.96	163.1	3.3, 9.1	0.608	1.5	2.20
Mes-CeTi-2.0	2:1	2:1.17	141.9	3.3, 9.1	0.529	1.5	2.24
Mes-CeO_2	1:0	–	134.6	3.3, 9.1	0.515	1.7	2.64

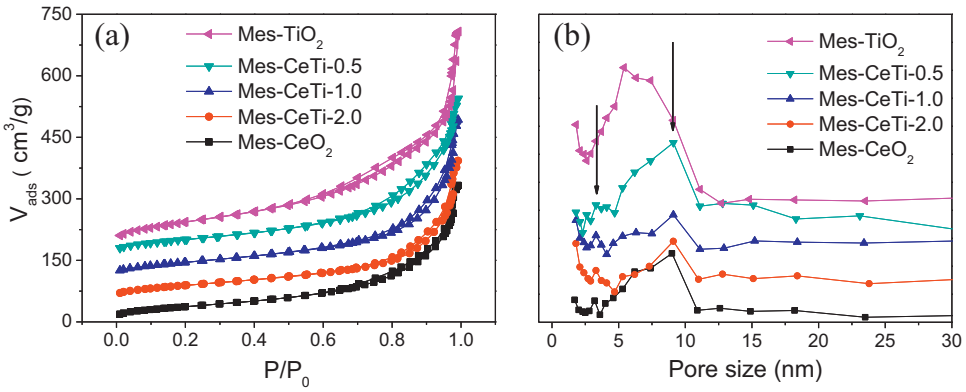

Fig. 3. N_2 adsorption/desorption isotherms (a) and corresponding pore size distribution curves (b) of Mes-TiO_2, Mes-CeTi-0.5, Mes-CeTi-1.0, Mes-CeTi-2.0, and Mes-CeO_2.

or transmission of the light scattered by the ordered mesopores implanted in the body of CeO_2-TiO_2 composites, and a similar effect has been verified in literature [32]. The band energy gap of above samples could be calculated by using $(\alpha h\nu)^n = k(h\nu - E_g)$, where α is the absorption coefficient, k is the parameter that related to the effective masses associated with the valence and conduction bands, n is $^1/_2$ for a direct transition, $h\nu$ is the absorption energy, and E_g is the band gap energy [41]. Plotting $(\alpha h\nu)^{1/2}$ versus $h\nu$ based on the spectral response in Fig. 5a give the extrapolated intercept corresponding to the E_g value (Fig. 5b). As shown in Table 1, the Mes-TiO_2 exhibits decreased E_g value (2.81 eV) with respect to that of commercial P25 (3.10 eV), which is consistent with the DRS result. Moreover, the optical band gap energies of the Mes-CeTi-0.5, Mes-CeTi-1.0, and Mes-CeTi-2.0 (2.16, 2.20, and 2.25 eV, respectively) display obvious red-shifts compared to that of Mes-TiO_2 (2.83 eV) and Mes-CeO_2 (2.61 eV). The results of this study therefore indicate that the enhanced ability to absorb visible-light of these ordered mesoporous CeO_2-TiO_2 composites makes them a promising photocatalyst for solar-driven applications.

The surface chemical state of Ce, Ti, and O in all samples was also investigated by XPS analysis. Ce 3d spectra of Mes-CeO_2 and three ordered mesoporous CeO_2-TiO_2 composites are shown in Fig. 6a. The labels used in identifying Ce 3d XPS peaks were established by Burroughs et al. [42], where ν and u indicate the spin-orbit coupling $3d_{5/2}$ and $3d_{3/2}$, respectively. The peaks denoted as ν', ν'', and ν''' are contributed by CeO_2, which can be respectively assigned to a mixture of Ce IV ($3d^94f^2$) O ($2p^4$), Ce IV ($3d^94f^1$) O ($2p^5$) and Ce IV ($3d^94f^0$) O ($2p^6$). The same peak assignment is applied to u structures. The ν'/u' doublet is ascribed to photoemission from Ce^{3+} cations [43]. Therefore, a mixture of Ce^{3+}/Ce^{4+} oxidation states exists on the surface of the Mes-CeO_2 and three ordered mesoporous CeO_2-TiO_2 composites, which was in good agreement with the studies of Fang et al. [44] and Gao et al. [45]. The surface concentrations of Ce^{3+} for Mes-CeO_2 and three ordered mesoporous CeO_2-TiO_2 composites evaluated by deconvolution of the XPS spectra are summarized in Table 2, it is worthy to note that Ce^{3+} concentrations in CeO_2-TiO_2 composites are much higher than that of Mes-CeO_2, suggesting that the introduction of TiO_2 into CeO_2 causes the partial reduction of Ce tetravalent cation [46].

Table 2
Summary of the XPS data for Mes-TiO_2, Mes-CeTi-0.5, Mes-CeTi-1.0, Mes-CeTi-2.0, Mes-CeO_2 and commercial P25.

Samples	$Ce^{3+}/(Ce^{3+}+Ce^{4+})$ (%)	OOH/OT (%)
Mes-TiO_2	–	34.6
Mes-CeTi-0.5	31.1	46.7
Mes-CeTi-1.0	28.9	42.1
Mes-CeTi-2.0	28.8	44.9
Mes-CeO_2	21.2	40.3
Commercial P25	–	29.1

The binding energies of Ti $2p_{1/2}$ and Ti $2p_{3/2}$ in both commercial P25 and Mes-TiO_2 are about 464.4 and 458.4 eV, respectively (Fig. 6b). Meanwhile, the presence of CeO_2 in composites shows no significant influence on the Ti2p binding energies which vary at most within ±0.3 eV. This indicates that Ti exists as Ti^{4+} in all samples, which agreed well with the values reported in the literature [44,47]. It can be also observed from Fig. 6b that the Ti 2p XPS peaks became broader after the introduction of CeO_2, which was attributed to the heterogeneous environments of Ti^{4+} in CeO_2-TiO_2 composites [44]. The surface Ce/Ti molar ratios derived from XPS for three ordered mesoporous CeO_2-TiO_2 composites are listed in Table 1, it can be seen that the results are in good agreement with the ratios in initial mixture.

Fig. 6c shows the O1s XPS spectra and the deconvolution results of all samples. The O1s XPS spectra appear broad, which can be deconvoluted into three distinct peaks: the one with lower binding energy is assigned to lattice oxygen in the metal oxides, the next is ascribed to chemisorbed oxygen or/and weakly bonded oxygen species, and the third peak at the highest binding energy is due to surface oxygen by hydroxyl species and/or adsorbed water species on the surface [38,45,48]. Based on the area integral of the three peaks respectively corresponding to lattice oxygen (OL), chemisorbed oxygen (OC) and surface oxygen (OS) of O 1s photoemissions, the ratio of OC to OT (OT = OL + OC + OS) for all samples was calculated as shown in Table 2. It can be noticed that the introduction of CeO_2 species can effectively enhance the chemisorbed oxygen on the surface of the CeO_2-TiO_2 composite. Because of the ordered mesostructure and high specific surface area, the Mes-TiO_2 possesses higher ratio of OC/OT than that of commercial P25.

3.2. Photoreduction of CO_2 under simulated solar irradiation

The photocatalytic activity of Mes-CeTi-0.5, Mes-CeTi-1.0, Mes-CeTi-2.0, Mes-TiO_2, Mes-CeO_2, and commercial P25 was evaluated in the reduction of CO_2 with H_2O under simulated solar irradiation. Fig. 7 shows the evolution of main products (CO and CH_4) as functions of irradiation time over all photocatalysts. It can be seen that the yields of CO and CH_4 are increased with the irradiation time for all photocatalysts, and three ordered mesoporous CeO_2-TiO_2 composites exhibit higher photocatalytic activity than Mes-TiO_2 as well as Mes-CeO_2, suggesting that CeO_2 addition can enhance the photocatalytic efficiency of pure mesoporous TiO_2. Moreover, the ordered mesoporous CeO_2-TiO_2 composites show a much higher level of activity than that of commercial P25.

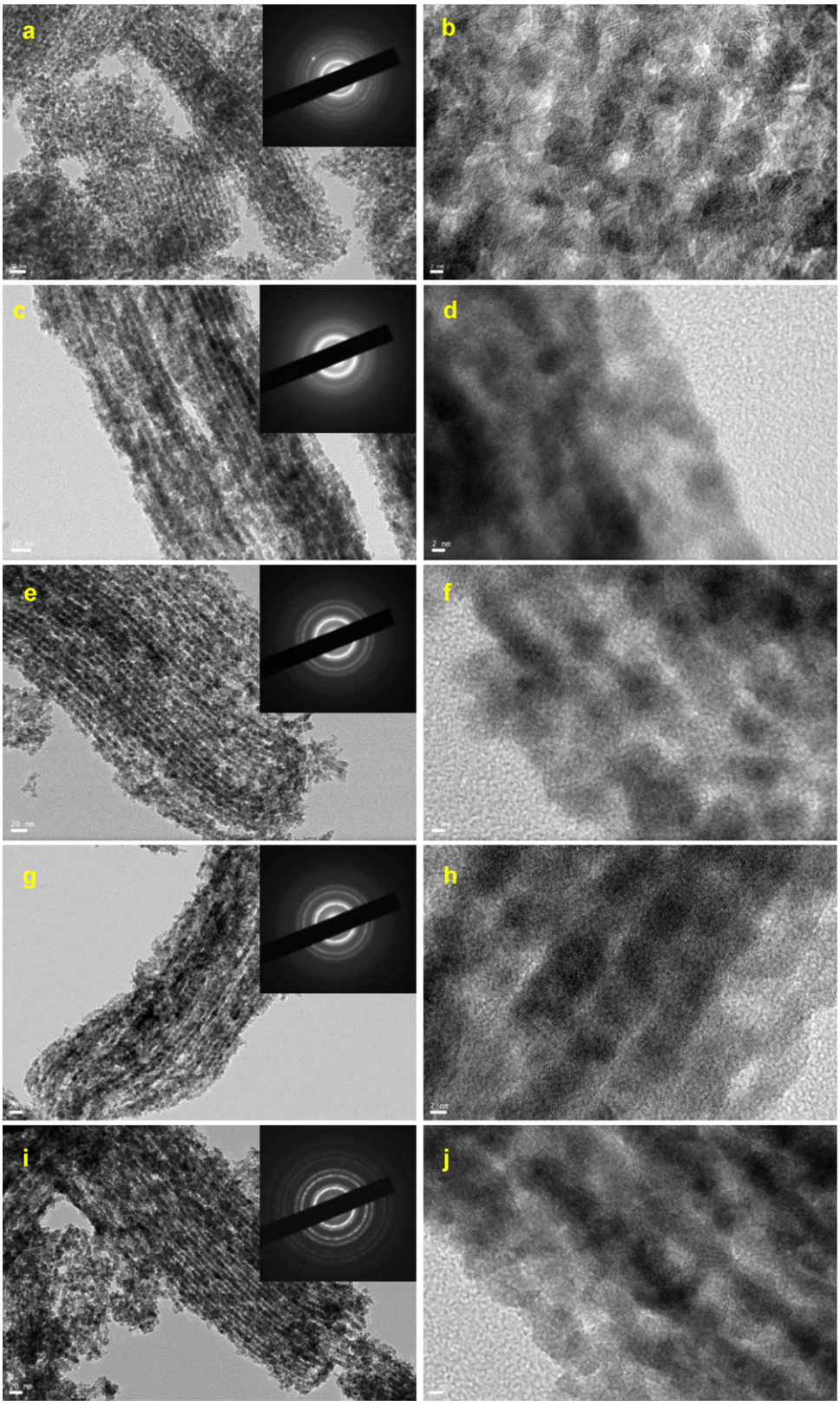

Fig. 4. TEM (left) and HRTEM (right) images of (a, b) Mes-TiO_2, (c, d) Mes-CeTi-0.5, (e, f) Mes-CeTi-1.0, (g, h) Mes-CeTi-2.0, (i, j) Mes-CeO_2.

The enhanced photocatalytic performance for these CeO_2-TiO_2 composites can be ascribed to their unique structure with a variety of favorable properties. First, ordered mesoporous architecture with large surface area and 2D open-pore system makes facile the reactant diffusion into the bulk of catalyst and hence provide fast intraparticle molecular transfer. Second, the introduction of CeO_2 species in composites can effectively extend the spectral response from UV to visible area owing to the CeO_2-photosensitization. In

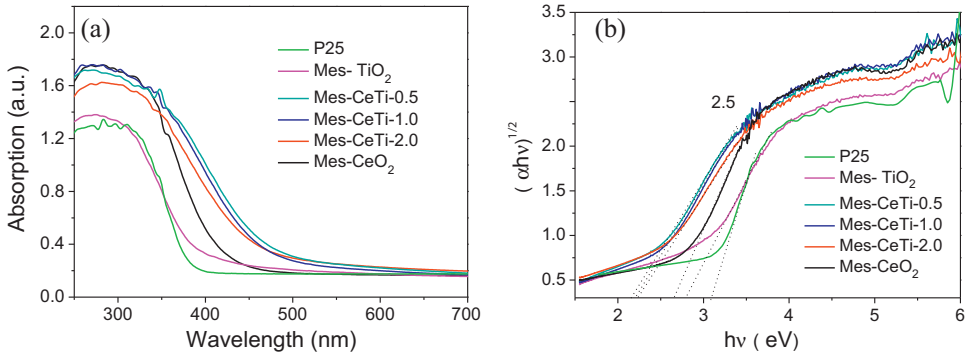

Fig. 5. (a) UV-vis diffuse reflectance spectra (DRS) and (b) the optical absorption edges of the Mes-TiO_2, Mes-CeTi-0.5, Mes-CeTi-1.0, Mes-CeTi-2.0, Mes-CeO_2 and commercial P25.

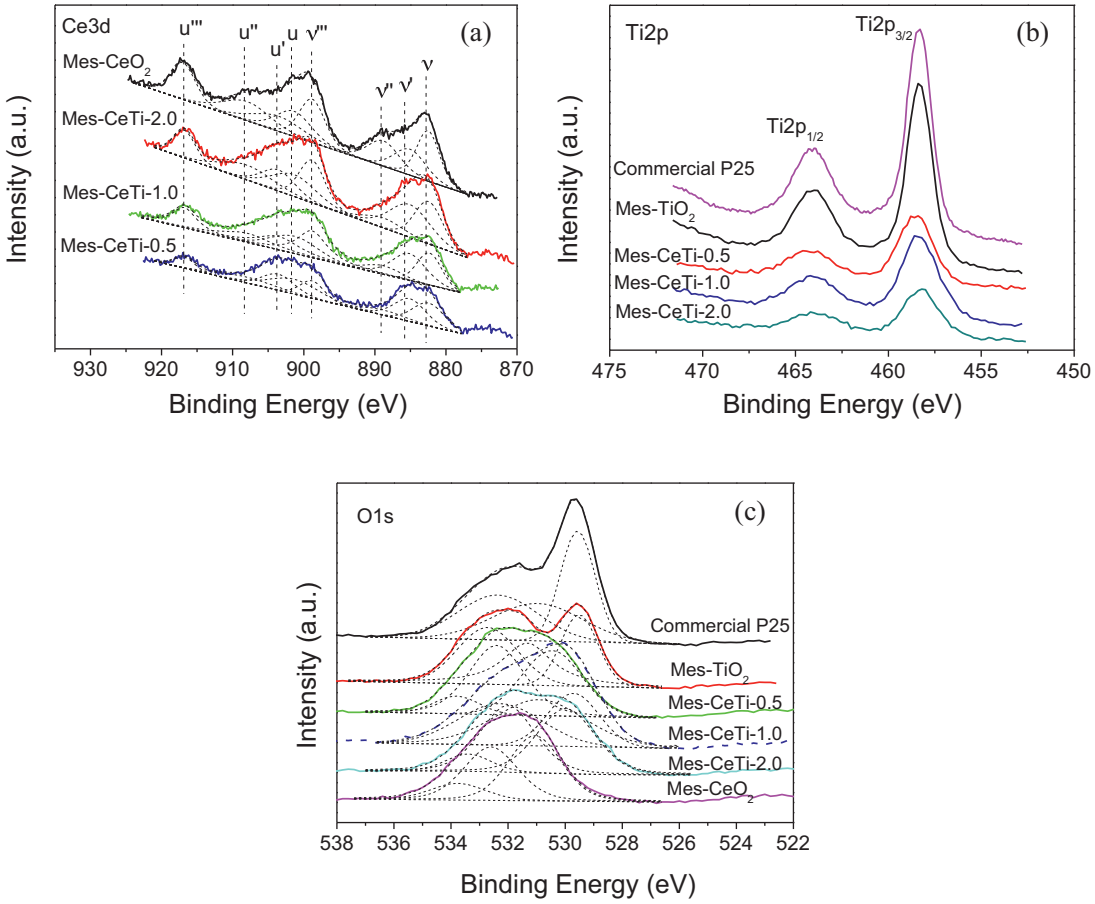

Fig. 6. (a) Ce 3d, (b) Ti 2p, and (c) O 1s XPS spectra of the Mes-TiO_2, Mes-CeTi-0.5, Mes-CeTi-1.0, Mes-CeTi-2.0, Mes-CeO_2 and commercial P25.

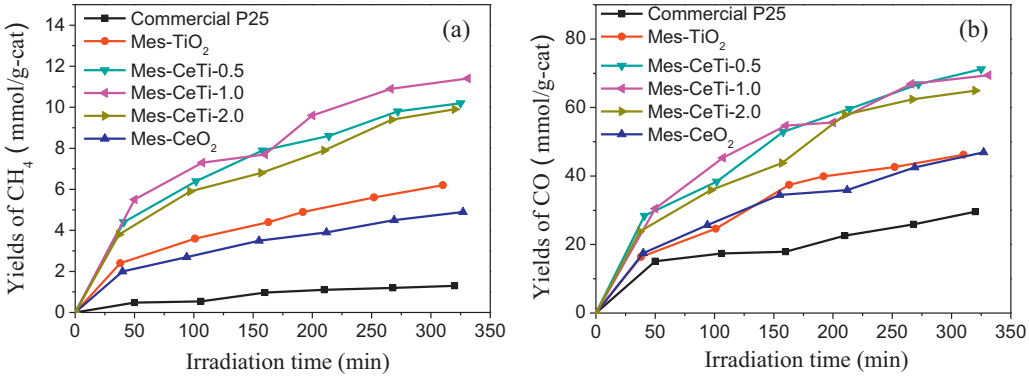

Fig. 7. Yields of CH_4 (a) and CO (b) as functions of irradiation time over all photocatalysts.

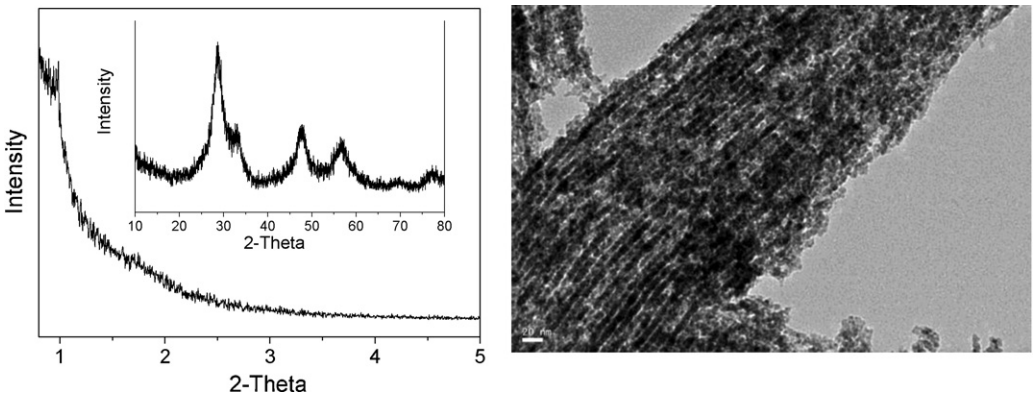

Fig. 8. XRD patterns (left) and TEM image (right) of the representative Mes-CeTi-1.0 sample after photocatalytic test.

our experiment, the 300 W Xe arc lamp excitation spectrum contains about 50% visible-light which is greatly contributed to the high photocatalytic efficiency for the ordered mesoporous CeO_2-TiO_2 composites in the reduction of CO_2 with H_2O. At the same time, the photogenerated electrons in the TiO_2 can drift to the CeO_2 under the inner electric field between CeO_2 and TiO_2 because of the energy band bending in space charge region, it is more helpful for the separation of photogenerated electron-hole pairs in TiO_2, resulting in the improvement of photocatalytic activity under solar irradiation. Finally, XPS analysis confirms that the CeO_2 addition can greatly enhance the surface chemisorbed oxygen species of the ordered mesoporous CeO_2-TiO_2 composites, these oxygen species can easily capture electrons and yield surface oxygen radicals with excellent reduction capability. Also, the existence of mixture of Ce^{3+}/Ce^{4+} oxidation states on the surface of CeO_2-TiO_2 composites denote that the partial metal in composites is not fully oxidized, so that Ce^{3+} can interact with holes and prevent the combination of photogenerated electrons and holes, resulting in a higher quantum efficiency of photocatalytic reaction.

In addition, in order to investigate the structural stability of the ordered mesoporous CeO_2-TiO_2 composites in photocatalytic reaction in the presence of H_2O, we have characterized the structure of these ordered mesoporous CeO_2-TiO_2 composites after photocatalytic test by XRD and TEM analysis. It was found that the structure of these used CeO_2-TiO_2 composites hasn't changed when compared with that of the corresponding fresh ones, indicating a good structural stability. Fig. 8 shows the XRD patterns and TEM image of the representative Mes-CeTi-1.0 sample after photocatalytic test.

4. Conclusions

In conclusion, we have demonstrated that ordered mesoporous CeO_2-TiO_2 composites with 2D hexagonal structure and varied compositions were synthesized via a simple nanocasting route. XRD, nitrogen sorption, and TEM results reveal that the obtained CeO_2-TiO_2 composites have ordered 2D hexagonal mesostructures with high specific surface area and hierarchical porosity. Introduction of CeO_2 species to TiO_2 can effectively extend the spectral response from UV to visible area and enhance the surface chemisorbed oxygen species of the ordered mesoporous CeO_2-TiO_2 composites, which are confirmed by UV-vis and XPS analysis. Due to the special composition and structure, the ordered mesoporous CeO_2-TiO_2 composites exhibited an excellent photocatalytic activity in the photoreduction of CO_2 with H_2O under simulated solar irradiation.

Acknowledgments

This work was supported by China Postdoctoral Science Foundation Funded Project (Grant No. 20100480534), China Postdoctoral Science Foundation Special Funded Project (Grant No. 201104236), and the National Natural Science Foundation of China (Grant No. 21103024).

References

[1] J.D. Figueroa, T. Fout, S. Plasynski, H. McIllvrid, P.D. Srivastava, International Journal of Greenhouse Gas Control 2 (2008) 9.
[2] T. Seki, Y. Kokubo, S. Ichikawa, T. Suzuki, Y. Kayaki, T. Ikariya, Chemical Communications (2009) 349.
[3] S. Liu, Z. Zhao, Z. Wang, Photochemical & Photobiological Sciences 6 (2007) 695.
[4] O.K. Varghese, M. Paulose, T.J. LaTempa, C.A. Grimes, Nano Letters 9 (2009) 731.
[5] Y. Li, W.N. Wang, Z. Zhan, M.H. Woo, C.Y. Wu, P. Biswas, Applied Catalysis B: Environmental 100 (2010) 386.
[6] M.A. Fox, M.T. Dulay, Chemical Reviews 93 (1993) 341.
[7] M. Anpo, H. Yamashita, Y. Ichihashi, S. Ehara, Journal of Electroanalytical Chemistry 396 (1995) 21.
[8] P. Pathak, M.J. Meziani, Y. Li, L.T. Cureton, Y.P. Sun, Chemical Communications (2004) 1234.
[9] K. Koci, L. Obalova, L. Matejova, D. Placha, Z. Lacny, J. Jirkovsky, O. Solcova, Applied Catalysis B: Environmental 89 (2009) 494.
[10] I.H. Tseng, W.C. Chang, J.C.S. Wu, Applied Catalysis B: Environmental 37 (2002) 37.
[11] I.H. Tseng, J.C.S. Wu, Catalysis Today 97 (2004) 113.
[12] P. Pathak, M.J. Meziani, L. Castillo, Y.P. Sun, Green Chemistry 7 (2005) 667.
[13] Q.H. Zhang, W.D. Han, Y.J. Hong, J.G. Yu, Catalysis Today 148 (2009) 335.
[14] K. Koci, K. Mateju, L. Obalova, S. Krejcikova, Z. Lacny, D. Placha, L. Capek, Applied Catalysis B: Environmental 96 (2010) 239.
[15] H. Yamashita, Y. Fujii, Y. Ichihashi, S.G. Zhang, K. Ikeue, D.R. Park, K. Koyano, T. Tatsumi, M. Anpo, Catalysis Today 45 (1998) 221.
[16] R. van Grieken, J. Aguado, M.J. Lopez-Munoz, J. Marugan, Journal of Photochemistry and Photobiology A: Chemistry 148 (2002) 315.
[17] X.H. Xia, Z.J. Jia, Y. Yu, Y. Liang, Z. Wang, L.L. Ma, Carbon 45 (2007) 717.
[18] H.C. Yang, H.Y. Lin, Y.S. Chien, J.C.S. Wu, H.H. Wu, Catalysis Letters 131 (2009) 381.
[19] K. Vinodgopal, P.V. Kamat, Environmental Science and Technology 29 (1995) 841.
[20] L.X. Cao, H.B. Wan, L.H. Huo, S.Q. Xi, Journal of Colloid and Interface Science 244 (2001) 97.
[21] L.R. Hou, C.Z. Yuan, Y. Peng, Journal of Hazardous Materials 39 (2007) 310.
[22] C.H. Wang, C.L. Shao, X.T. Zhang, Y.C. Liu, Inorganic Chemistry 48 (2009) 7261.
[23] J.H. Pan, W.I. Lee, Chemistry of Materials 18 (2006) 847.
[24] V. Puddu, R. Mokaya, G.L. Puma, Chemical Communications (2007) 4749.
[25] I. Paramasivam, Y.C. Nah, C. Das, N.K. Shrestha, P. Schmuki, Chemistry - A European Journal 16 (2010) 8993.
[26] J.C. Yu, L. Wu, J. Lin, P. Li, G. Li, Chemical Communications (2003) 1552.
[27] M.C. Hsu, I.C. Leu, Y.M. Sun, M.H. Hon, Journal of Crystal Growth 285 (2005) 642.
[28] Y. Xie, G. Ali, S.H. Yoo, S.O. Cho, ACS Applied Materials & Interfaces 2 (2010) 2910.
[29] W. Zhou, H.G. Fu, K. Pan, C.G. Tian, Y. Qu, P.P. Lu, C.C. Sun, Journal of Physical Chemistry C 112 (2008) 19584.
[30] L.L. Peng, T.F. Xie, Y.C. Lu, H.M. Fan, D.J. Wang, Physical Chemistry Chemical Physics 12 (2010) 8033.

[31] S. Pavasupree, Y. Suzuki, S. Pivas-Art, S. Yoshikawa, Journal of Solid State Chemistry 178 (2005) 128.
[32] H. Liu, M. Wang, Y. Wang, Y. Liang, W. Cao, Y. Su, Journal of Photochemistry and Photobiology A: Chemistry 223 (2011) 157.
[33] W. Zhou, K. Liu, H. Fu, K. Pan, L. Zhang, L. Wang, C. Sun, Nanotechnology 19 (2008) 035610.
[34] G. Dutta, U.V. Waghmare, T. Baidya, M.S. Hegde, K.R. Priolkar, P.R. Sarode, Chemistry of Materials 18 (2006) 3249.
[35] S. Watanabe, X. Ma, C. Song, Journal of Physical Chemistry C 115 (2009) 14249.
[36] Y. Ren, Z. Ma, P.G. Bruce, Chemical Society Reviews 41 (2012) 4909.
[37] Z. Bian, J. Zhu, S. Wang, Y. Cao, X. Qian, H. Li, Journal of Physical Chemistry C 112 (2008) 6258.
[38] G. Li, D. Zhang, J.C. Yu, Physical Chemistry Chemical Physics 11 (2009) 3775.
[39] Y.G. Wang, F.Y. Zhang, Y.Q. Wang, J.W. Ren, C.L. Li, X.H. Liu, Y. Guo, Y.L. Guo, G.Z. Lu, Materials Chemistry and Physics 115 (2009) 649.
[40] J.C. Yu, X.C. Wang, X.Z. Fu, Chemistry of Materials 16 (2004) 1523.
[41] M. Yoon, M. Seo, C. Jeong, J.H. Kang, K.S. Jeon, Chemistry of Materials 17 (2005) 6069.
[42] P. Burroughs, A. Hamnett, A.F. Orchard, G. Thornton, Journal of the Chemical Society, Dalton Transactions 17 (1976) 1686.
[43] C.M. Ho, J.C. Yu, T. Kwong, A.C. Mak, S.Y. Lai, Chemistry of Materials 17 (2005) 4514.
[44] J. Fang, X. Bi, D. Si, Z. Jiang, W. Huang, Applied Surface Science 253 (2007) 8952.
[45] X. Gao, Y. Jiang, Y. Zhong, Z. Luo, K. Cen, Journal of Hazardous Materials 174 (2010) 734.
[46] S. Watanabe, X. Ma, C. Song, Journal of Physical Chemistry C 113 (2009) 14249.
[47] Z. Wu, R. Jin, H. Wang, Y. Liu, Catalysis Communications 79 (2008) 347.
[48] J. Zhu, J. Yang, Z.F. Bian, J. Ren, Y.M. Liu, Y. Cao, H.X. Li, H.Y. He, K.N. Fan, Applied Catalysis B: Environmental 76 (2007) 82.